Gas-Surface Interaction Models in Hypersonic Flows

Carlos Teixeira
carlos.c.teixeira@ist.utl.pt

Instituto Superior Técnico, Lisboa, Portugal

December 2015

Abstract

This thesis consists on the implementation of catalycity in SPARK. SPARK is an aerothermodynamics code that solves the reacting Navier-Stokes equations. It is used to simulate re-entry flows of space vehicles. SPARK is developed and maintained at IPFN. Until then SPARK neglected heterogeneous reactions (fluid/solid interaction) through which 2 atoms, mediated by the surface, recombine, releasing energy into the vehicle. However, this capability is standard in similar codes. Catalyticy has an effect on the composition of the flow and plays a pivotal role on the heat flux into the space-ship. A model that describes catalycity macroscopically has been introduced. In this model the recombination at the wall of two dissociated species is characterized by a single parameter that can be either constant or temperature dependent. That required a suitable improvement of the mass and energy balance equations between the fluid flow and the wall. The results from various simulations were compared with other numerical codes and experimental data. Furthermore, the first stage of the implementation of a more advanced model, termed FRSC, that takes into account ablation and pyrolysis phenomenon has been achieved. This initial formulation describes microscopically, and in great detail, the heterogeneous chemical reactions on the particular case of no gas flow; and serves as the foundation for the final implementation of the FRSC on a flow governed by the full reacting Navier-Stokes equations.
Keywords: TPS, catalycity, SPARK, hypersonic flow, aerothermodynamics

1. Introduction

Space vehicles enter the Earth at near orbital ($V_\infty = 7.9\,\frac{\text{km}}{\text{s}}$) speeds, relative to the atmosphere [4]. In this hypersonic flow regime a strong shock-wave is formed upstream of the spacecraft, wherein the flow slows down to subsonic speeds. The total energy associated with such high velocities ($\approx \frac{1}{2}mV^2$) is partially converted into internal energy. As a first approximation if we assume that all this energy is absorbed by the vehicle:

$$Q = \frac{1}{2}mV^2 \Leftrightarrow \frac{Q}{m} = \frac{V^2}{2}$$
$$V_\infty \approx 7.9\,\frac{\text{km}}{\text{s}} : \frac{Q}{m} = 31\,401\,\frac{\text{kJ}}{\text{kg}} \qquad (1)$$

Where Q is the total (kinetic) energy, m is the mass of the spaceship and V its velocity.

Few materials could withstand this level without disintegrating [5]. Admittedly this is a crude analysis, and not all the energy is absorbed by the vehicle. However these concise calculation helps evidencing why heat loading is a key parameter for the design of entry spacecraft. Effectively, the surface of such vehicles must be equipped with a Thermal Protection System (TPS) designed to sustain heat loads of this magnitude without endangering the underlying structure [3]. For re-entry flows, the diffusion heat flux due to mass gradients is of the same order of the convective heating fluxes due to temperature gradients and therefore a modelling of catalycity is essential.

1.1. Objectives

This work aims at improving the capabilities of the SPARK code.

SPARK is a code capable of hypersonic re-entry simulations. It has been developed and is maintained at IPFN - IST. SPARK takes into account finite-rate chemistry and vibrational non-equilibrium effects by solving the reacting Navier-Stokes equations. It is written in Fortran 03/08 language via oriented object programming.

Before the current work, SPARK did not have the capability to account for catalycity in re-entry simulations. It neglected the phenomenon by assuming the wall of a re-entry vehicle is indifferent to surface reactions. This limited the application of SPARK to simulations where catalycity was not expected to play a significant role. When catalycity is relevant, it primarily affects the heat flux into the vehicle and the gas composition near the surface.

Hence, the first objective consisted in implementing in SPARK a versatile catalytic capability that could account for recombination of N_2 and O_2, essential in Earth re-entry.
The general approach followed is similar to what other codes have implemented in the past, where catalycity is treated phenomenologically by which surface reactions are modelled from a macroscopic point of view. Here a surface efficiency γ is defined, which quantifies the ratio of N and O atoms that recombine in the wall.
The second objective consisted in a preliminary formulation of the Finite-Rate Surface Chemistry (FRSC) model. The FRSC can be viewed as a module that rigorously describes surface reactions, by accounting for the actual physical mechanisms by which they occur. This module is implemented as a boundary condition to the reacting Navier-Stokes equations on state-of-the-art CFD codes as DPLR [6] and LeMANS [1]. On this work however, a stand-alone code, decoupled from the fluid flow was developed, as a first step for the full implementation in SPARK.

2. Physical models

When a reactive gas is considered, a boundary condition must by specified to model the species mass fractions at the wall. These models are often referred as *wall catalycity*.

2.1. Catalytic Models Available

Several different approaches can be used to describe wall catalycity:

Non-catalytic model: In this model the surface behaves as being indifferent to the gas flow. The impinging atoms on the vehicle wall do not recombine. No diffusion occurs. This was the only model originally implemented in SPARK.

Fully catalytic model: This model assumes all the incoming atoms recombine into molecules releasing heat into the surface, and thus providing an upper bound for the heat flux into the vehicle.

Partially catalytic model: This model assumes that only a fraction of the incoming atoms recombines at the wall. The first two models are therefore particular cases. This was the model implemented on SPARK. On this work it is referred as the Specified Reaction Efficiency (SRE) model.

Super catalytic model: This model imposes the composition at the wall to be equal to the free-stream composition.

The equilibrium wall model: This model assumes that the wall composition is the equilibrium composition at the wall pressure and temperature.

Finite-rate model: This model accounts for the actual chemical processes occurring on the surface. It is a very advanced model based on the actual microscopic steps involved in a surface reaction. On this work it is referred as the FRSC model.

2.2. Species boundary condition

The implementation of the partially catalytic model in SPARK starts with mass and energy balances at the fluid/surface interface:
By Fick's Law of diffusion, when in a given mixture there is a gradient of mass of a given species i , there will be a mass motion of this species in the direction opposite of the gradient as given by (2).

$$\mathbf{j}_i = -\rho D_i \nabla c_i \tag{2}$$

Where D_i is the diffusion coefficient of species i and ρ is the density of the mixture.
Given the direction n, normal to the surface on figure 1, the mass flux into the wall is given by (3).

$$(j_i)_{\text{w, into the wall}} = \left(\rho D_i \frac{\partial c_i}{\partial n}\right)_{\text{w}} \tag{3}$$

We are now in a position to derive the boundary condition. Referring to illustration 1, if we imagine a control volume that envelops the flow/surface interface, in steady state, the net rate of diffusion of species i to the surface must be balanced to the rate at which species i is being destroyed due to catalycity.

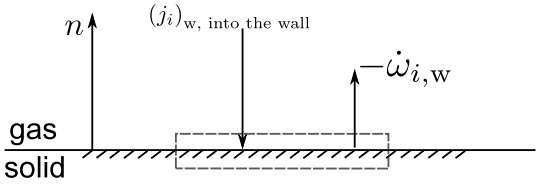

Figure 1: Mass wall balance of species i at the wall.

For this purpose, let $\dot{\omega}_{i,\text{w}}$ be the production of species i (mass of species i per second per unit area). Henceforth, at the wall, the rate at which species i diffuses into the wall must be balanced by the surface amount of its destruction, which given the definition above is $(-\dot{\omega}_{i,\text{w}})$:

$$\begin{aligned}(j_i)_{\text{w, into the wall}} &= (-\dot{\omega}_{i,\text{w}}) \Leftrightarrow \\ -\left(\rho D_i \frac{\partial c_i}{\partial n}\right)_{\text{w}} &= (\dot{\omega}_{i,\text{w}})\end{aligned} \tag{4}$$

2.3. Modelling the Source Terms $\dot{\omega}_{i,\text{w}}$

The specified reaction efficiency (SRE) model follows when one looks at the flow near a wall from

a macroscopic point of view. That is, we realize that near a wall there are some atoms impinging on it. Thus, it is natural to assume that from that amount of atoms only a portion will recombine into molecules, while the other part will be reflected. The fraction of incident atoms impinging on the surface that recombine is referred as recombination coefficient or reaction efficiency and defined as γ :

$$\gamma_i \equiv \frac{|M_i|}{|M_i^{\downarrow}|} \tag{5}$$

Where $|M_i^{\downarrow}|$ is the mass flux of atoms towards the surface, and $|M_i|$ is the mass flux of actual recombining atoms.
What is ultimately desired is an expression modelling the production term $\dot{\omega}_{i,\mathrm{w}}$, which should have units of mass of species i per second per unit area. The production term is in fact $|M_i|$ both from its description and units. The expression for the mass flux of atoms impinging on the surface, $|M_i^{\downarrow}|$, follows from kinetic theory [7], [12]:

$$M_i^{\downarrow} = c_{i,\mathrm{w}}\rho_{\mathrm{w}}\sqrt{\frac{R_i T_{\mathrm{w}}}{2\pi}}, \quad \left[\mathrm{kg\,m^{-2}\,s^{-1}}\right] \tag{6}$$

Catalycity in SPARK was implemented for air environments for which there are 3 reactions of interest [10]:

$$\begin{aligned} \mathrm{N} + \mathrm{N} &\longrightarrow \mathrm{N_2} \\ \mathrm{O} + \mathrm{O} &\longrightarrow \mathrm{O_2} \\ \mathrm{N} + \mathrm{O} &\longrightarrow \mathrm{NO} \end{aligned} \tag{7}$$

Amongst these, recombination of nitrogen oxide is less important than the other two [10] and was thus ignored. Given the definition for γ and also (6) and (7) the production terms for the incoming atoms are:

$$\begin{aligned} \dot{\omega}_{N,\mathrm{w}} &= -\gamma_N c_{N,\mathrm{w}}\rho_{\mathrm{w}}\sqrt{\frac{R_N T_{\mathrm{w}}}{2\pi}} \quad \left[\mathrm{kg\,m^{-2}\,s^{-1}}\right] \\ \dot{\omega}_{O,\mathrm{w}} &= -\gamma_O c_{O,\mathrm{w}}\rho_{\mathrm{w}}\sqrt{\frac{R_O T_{\mathrm{w}}}{2\pi}} \quad \left[\mathrm{kg\,m^{-2}\,s^{-1}}\right] \end{aligned} \tag{8}$$

The production terms for the products $\mathrm{N_2}$ and $\mathrm{O_2}$ follow from (8) and the principle of element conservation [7]. The net number of atoms produced regardless of their molecular arrangement must equal 0. For the 2 reactions considered this states, in terms of mass:

$$\begin{aligned} \dot{\omega}_{N_2,\mathrm{w}} + \dot{\omega}_{N,\mathrm{w}} = 0 \Leftrightarrow \dot{\omega}_{N_2,\mathrm{w}} = \gamma_N c_{N,\mathrm{w}}\rho_{\mathrm{w}}\sqrt{\frac{R_N T_{\mathrm{w}}}{2\pi}} \\ \dot{\omega}_{O_2,\mathrm{w}} + \dot{\omega}_{O,\mathrm{w}} = 0 \Leftrightarrow \dot{\omega}_{O_2,\mathrm{w}} = \gamma_O c_{O,\mathrm{w}}\rho_{\mathrm{w}}\sqrt{\frac{R_O T_{\mathrm{w}}}{2\pi}} \end{aligned} \tag{9}$$

2.4. The recombination coefficient, γ
The recombination coefficient γ represents an overall efficiency and is not based on a single chemical process which, in reality, takes place. For this reason, values for γ are normally obtained from experiments. In SPARK the user can choose to set γ_N and γ_O to a constant value (e.g., $\gamma = 0$, 0.01, 0.5 etc.) which he finds fit or he can choose pre-defined correlations in the form $\gamma = \gamma(T)$ where each point on the wall has a different γ according with T_{w}.
What is often done is to set $\gamma = 1$, which defaults to a fully-catalytic model, and provides an upper limit for the heat-flux.

2.5. Surface Energy Balance
Temperature is also a dependent variable and thus requires appropriate boundary conditions. It is often assumed that the vehicle surface can maintain a constant temperature T_{w}, but rare are the situations this is a valid assumption. In alternative, the temperature is allowed to vary along the surface but is dictated by an energy balance at the wall. As illustrated on figure 2, energy arrives at the surface via different mechanisms. Convection, q_{conv} originates from temperature gradients. Due to the gradients of mass of each species, diffusion contributes with as many terms as the N_s different species in the gas. The term $\dot{q}_{\text{rad-out}}$ accounts for the re-radiation by the surface assuming a constant emissivity ϵ. In SPARK the value used was $\epsilon = 0.85$. The heat conduction into the vehicle ($\dot{q}_{\text{cond}}$) and the radiation received from the gas are often ignored. In that case, at (10), the surface is then said to be at radiative equilibrium. This was the approach implemented in SPARK which can, in alternative, use a constant wall temperature T_{w}.

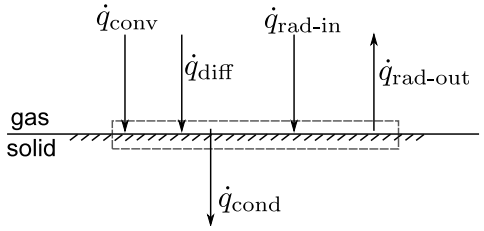

Figure 2: Wall energy balance. Heat fluxes over the catalytic surface.

$$\underbrace{\left(k\frac{\partial T}{\partial n}\right)_{\mathrm{w}}}_{\dot{q}_{conv}} + \underbrace{\left(\sum_{i=1}^{N_s} h_i \rho D_i \frac{\partial c_i}{\partial n}\right)_{\mathrm{w}}}_{\dot{q}_{diff}} = \underbrace{\epsilon\sigma T_{\mathrm{w}}^4}_{\dot{q}_{rad-out}} \tag{10}$$

3. Implementation of the species mass balance

Expression (4) is the analytical boundary condition resulting from the wall mass balance. For the numerical implementation, we proceed with a 1^{st} order approximation of the gradient as given by:

$$\left(\frac{\partial c_i}{\partial n}\right)_{\mathrm{w}} = \frac{(c_i)_{\mathrm{i}} - (c_i)_{\mathrm{w}}}{\Delta n} \tag{11}$$

where $(c_i)_{\mathrm{i}}$ and $(c_i)_{\mathrm{w}}$ are the mass fractions at the internal cell closest to the wall and the wall respectively, and Δn is the distance between the cell and the wall as figure 3 illustrates.

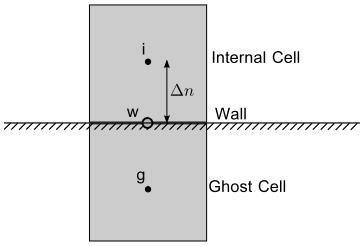

Figure 3: Finite volume cells at the Wall.

Inserting (11) into (4), and noting that (4) is valid for every instant in time:

$$c^n_{i,\mathrm{w}} = c^n_{i,\mathrm{i}} + \dot{\omega}^n_{i,\mathrm{w}} \cdot \left(\frac{\Delta n}{\rho_{\mathrm{w}} D_{i,\mathrm{w}}} \right)^n \tag{12}$$

where the superscript n indicates a discretized time instant and the subscripts i and w indicate evaluation at the first internal cell and the wall respectively.
The unknown of the above equation is the wall mass fraction of species i, $c_{i,\mathrm{w}}$. However, in general, the production terms $\dot{\omega}_{i,\mathrm{w}}$, depend not only on the mass fraction of $c^n_{i,\mathrm{w}}$ but also on other species mass fractions $c^n_{k,\mathrm{w}}$, as equation (13) highlights.

$$\dot{\omega}^n_{i,\mathrm{w}} = f(c^n_{k,\mathrm{w}});\ k = 1,\ ...,\ N_s; \tag{13}$$

Where N_s is the number of species.
Therefore, to account for this coupling, we proceed with the implicitation of (12). Following the implicit approach, the production terms $\dot{\omega}^n_{i,\mathrm{w}}$ are discretized with a Taylor expansion of 1^{st} order on the wall mass fractions around the previous time interval $n-1$. Because the function has several variables, namely N_s variables:

$$\dot{\omega}^n_{i,\mathrm{w}} = \dot{\omega}^{n-1}_{i,\mathrm{w}} + \sum_{j=1}^{N_{\mathrm{S}}} \left(\frac{\partial \dot{\omega}_{i,\mathrm{w}}}{\partial c_{j,\mathrm{w}}} \right)^{n-1} \cdot \left(c^n_{i,\mathrm{w}} - c^{n-1}_{i,\mathrm{w}} \right) \tag{14}$$

Where the derivatives of the mass source terms with respect to the species mass fractions $\partial \dot{\omega}_{i,\mathrm{w}} / \partial c_{j,\mathrm{w}}$ need to be computed analytically what requires the expressions for $\dot{\omega}_{i,\mathrm{w}}$. Inserting (14) in (12) it is possible to arrive, after some algebraic manipulation, at a system of algebraic equations where all mass fractions $c_{i,\mathrm{w}}$ of all species at the wall are solved simultaneously:

$$[A] \cdot \left\{ c^n_{i,\mathrm{w}} \right\} = \{b\} \tag{15}$$

with

$$A_{ij} = \delta_{ij} - \alpha_i^{n-1} \left(\frac{\partial \dot{\omega}_{i,\mathrm{w}}}{\partial c_{j,\mathrm{w}}} \right)^{n-1}$$

$$b = c^n_{i,\mathrm{i}} + \left[\dot{\omega}^{n-1}_{i,\mathrm{w}} - \sum_{j=1}^{N_{\mathrm{S}}} c^{n-1}_{i,\mathrm{w}} \cdot \left(\frac{\partial \dot{\omega}_{i,\mathrm{w}}}{\partial c_{j,\mathrm{w}}} \right)^{n-1} \right] (\alpha_i)^{n-1}$$

Where the term:

$$\alpha_i^{n-1} = \left(\frac{\Delta n}{\rho_{\mathrm{w}} D_{i,\mathrm{w}}} \right)^{n-1}$$

has been introduced for convenience in the derivation and δ_{ij} is the Kronecker delta function.
In summary, on a given iteration n, we want to compute the wall mass fractions of all the N_s species. The information available at that time is all the unknowns at the previous time $n-1$, as well as the variables (including the mass fractions) on all internal cells, $c_{i,\mathrm{i}}$.

4. Implementation of the surface energy balance

On equation (13), it was assumed that the production terms $\dot{\omega}_{i,\mathrm{w}}$ depend only on the mass fractions. As seen previously they in fact also depend on temperature as emphasized on (16). For an isothermal wall case, this dependence does not need to be taken into account on the implicitation since T_{w} is prescribed along the entire surface and at all time instants.

$$\dot{\omega}^n_{i,\mathrm{w}} = f(c^n_{k,\mathrm{w}},\ T^n_{\mathrm{w}});\ k = 1,\ ...,\ N_s; \tag{16}$$

For the surface energy balance (SEB) the temperature at the wall T_{w} is evaluated via (10) but there the diffusion terms require the derivative of the mass fractions at the wall to be already known. Since the production terms depend on T_{w} and they are needed to find the mass fractions at the wall this gives rise to another impasse. SPARK deals with this coupling explicitly. The algorithm implement is exposed on figure 4.
After a particular CFD iteration n, all the variables in all the cells are known. In particular the temperature T^n_{i} and the mass fraction of each species $c^n_{i,\mathrm{w}}$ are known at the first internal cell i. Also available are the wall values of this quantities from the previous iteration $n-1$: T^{n-1}_{w} and $c^{n-1}_{i,\mathrm{w}}$. The first step is to compute the new mass fractions at the wall $c^n_{i,\mathrm{w}}$ by solving (15) previously discussed; for that it is initially assumed the temperature at the wall to be T^{n-1}_{w}. After the previous step, all mass fractions at the wall of all species at time level n are provisionally known.
The second step consists in extracting a new T^n_{w} by solving the surface energy balance (10). Because

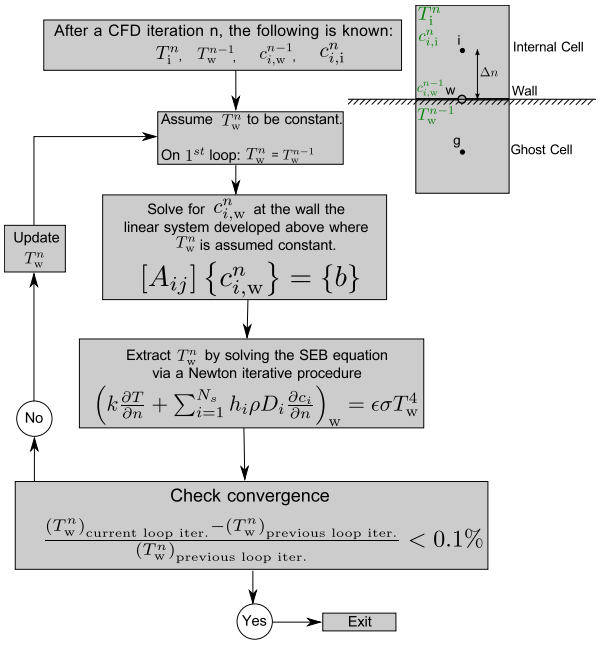

Figure 4: Algorithm of the explicit approach implemented on SPARK to deal with surfaces in radiative equilibrium, where T_w is not known a priori.

the equation is non-linear, it requires a Newton iterative procedure. This temperature is then compared with the temperature initially used to solving for the mass fractions $c_{i,w}^n$. If the results didn't converge, the new T_w^n is fed back to the linear system and the loop continues until the convergence criterion is met.

5. Results

To assess the credibility of the implementation of catalycity, SPARK results are compared with experimental data and computational simulations from similar codes. Temperature and mass fraction profiles as well as heat flux loading are compared because these are the variables most influenced by catalycity.

The test cases consisted in flows over sharp cones from Miller et al., 1994 [9] and over the blunt body Electre from Barbato et al., 1994 [2], Muylaert et al., 1998 [11] and Viviani et al., 2009 [13].

5.1. Sharp Cones

The cone has an axial length of 0.5 m and a semi-angle of 10°. The species considered were N_2, O_2, N, O and NO with the upstream conditions:

V_∞ [m/s]	T_∞ [K]	P_∞ [Pa]	c_{N_2} [-]	c_{O_2} [-]
8071	252.6	20.35	0.7371	0.2629

Table 1: Upstream conditions for the simulation over the sharp cone.

The mass fraction profiles of figure 5 show a good qualitative agreement but dubious quantitative agreement.

On the qualitative side, both the non catalytic and fully catalytic conditions constitute the upper and lower limits for the mass fractions respectively, with the intermediate catalycity efficiencies having, at every constant y_{normal} station, a value greater than the immediately higher catalytic γ value, which means there are no cross overs between the profiles of each different γ. Moreover, the O mass fraction slopes at the wall are positive which through equation (4) means that there is only destruction and never production of O at the wall. This is physically consistent with the catalytic model implemented that allows the forward reaction $O + O \longrightarrow O_2$ but never its inverse which produces O. Similarly, the slopes of mass fraction for O_2 (profiles for O_2 not shown), $\frac{\partial c_{o_2}}{\partial n}$, are negative since O_2 can be created at the wall, but never destroyed.

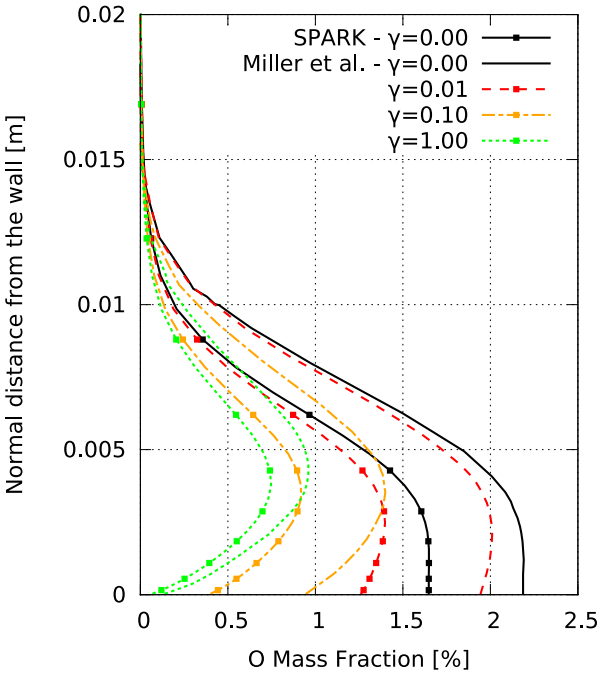

Figure 5: O mass fraction profiles normal to the cone surface at 0.5 m.(SEB boundary condition)

On the quantitative side, Miller et al. predicts 56% more c_O at the wall then SPARK for $\gamma = 0.01$, with the differences peaking 100% when $\gamma = 0.1$.

Amongst the differences between SPARK and Miller's CFD code, the procedure to compute enthalpy of each species is different. Because the specific enthalpy h_i enters the SEB equation (10), this can to some extent explain the differences.

5.2. Electre Probe

Electre is a standardized spherical-conical blunt body defined by an axial length of 0.4 m, a semi-

aperture cone angle of 4.6° and a nose radius of 0.035 m. The species considered were N_2, O_2, N, O and NO with the upstream conditions given by:

	T_∞, K	ρ_∞, $\frac{kg}{m^3}$	V_∞, $\frac{m}{s}$	c_{N_2}	c_{O_2}	c_O	c_{NO}	T_{wall}, K
Viviani	790	16.40E-4	5953	0.754	0.0367	0.1817	0.0272	300
Muylaert	795	5.450E-4	4930	0.773	0.2376	0	0	300
Barbato	$\frac{T=766.38}{T_V=3930}$	20.17E-4	5953	0.754	0.0367	0.1817	0.0272	343

Table 2: Upstream conditions for the Electre cases.

From a broad perspective, by inspecting figures 6, 7 and 8 we may immediately find that there is a good qualitative agreement and a decent quantitative agreement between the current SPARK and Barbato et al. results. For temperature, SPARK captures the same "S" like shape near the wall but overpredicts that local maximum by 8%. The profile seems to be shifted to the right. The discrepancies for $y_{\text{normal}} > 2\,\text{cm}$ are considered not to be born out of the catalytic model.

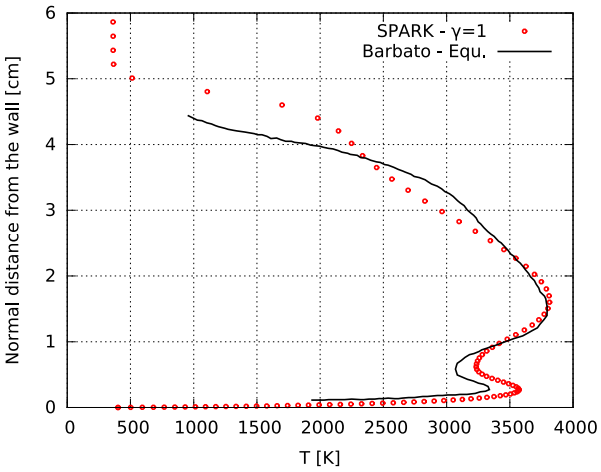

Figure 6: Temperature along the normal to Electre's wall at x = 0.1 m for $T_w = 343\,K$. Comparison of SPARK results with Barbato et al. [2]

There is also a very good agreement for the N_2 and N profiles. The biggest difference being the value and slope for c_{N_2} at the wall. Notice that the trends of N_2 and N are mirrored since the creation of N_2 occurs at the expense of N through $N + N \longrightarrow N_2$. The curves on figure 8 are nearly identical with the differences for $y_{\text{normal}} > 1\,\text{cm}$ being attributed to the distinct discretization schemes used in each code. In particular the slopes values at the wall are very similar, it would be thus expected that the predicted contributions of O for the diffusive heat-flux to be equal. This slopes are positive, indicating a mass flux of O into the wall, which is feeding the creation of O_2 via $O + O \longrightarrow O_2$.
Moving to the comparison of heat loads, on the reproduction of Viviani's results, SPARK underpredicts the heat flux along the entire length of the probe. It presents a total heat-flux 90% lower at the

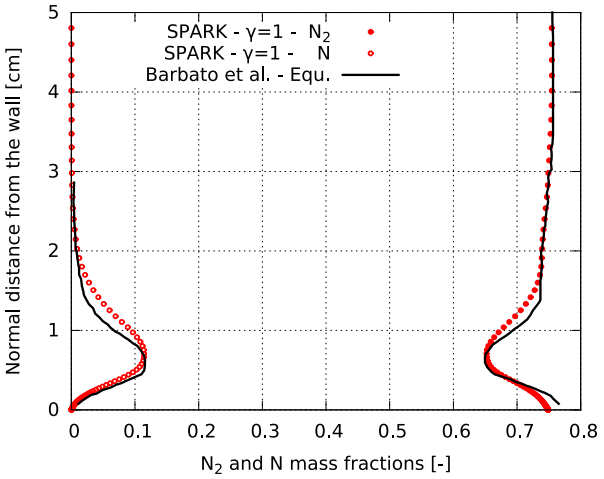

Figure 7: Mass fractions along the normal to Electre's wall at x = 0.1 m for $T_w = 343\,K$. Comparison of SPARK results with Barbato et al. [2].

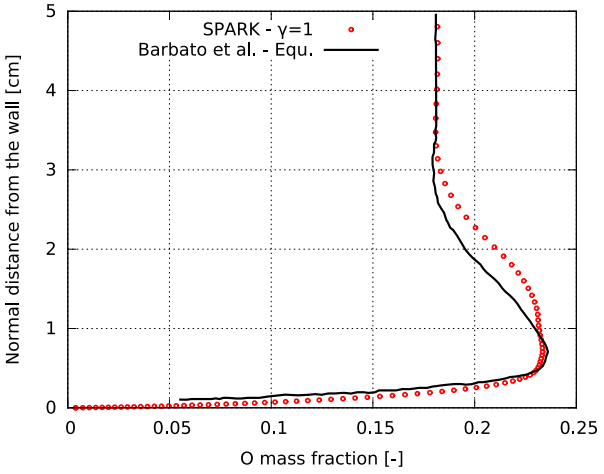

Figure 8: Mass fractions along the normal to Electre's wall at x = 0.1 m for $T_w = 343\,K$. Comparison of current results under SPARK with Barbato et al. [2].

nose of Electre and 50% lower at $\frac{x}{L} = 1$. Only the break-up of the total heat flux onto its constituent terms (i.e., convective and diffusive fluxes) would allow to better comprehend the origin of the discrepancy. Furthermore, the experimental data shows that SPARK predicts relatively well the heat flux on the spherical portion of Electre but not along its slope. Despite to this, the results have a very good qualitative agreement as they appear to just being shifted from one to another.
It should be added that the SPARK simulations were ran with thermal equilibrium while Viviani et al. assumed a two-temperature model. Also different was the procedure to compute the diffusion coefficient of all species, D_i. However, it is not believed the results would have suffered any consider-

able changes had the models been the same.

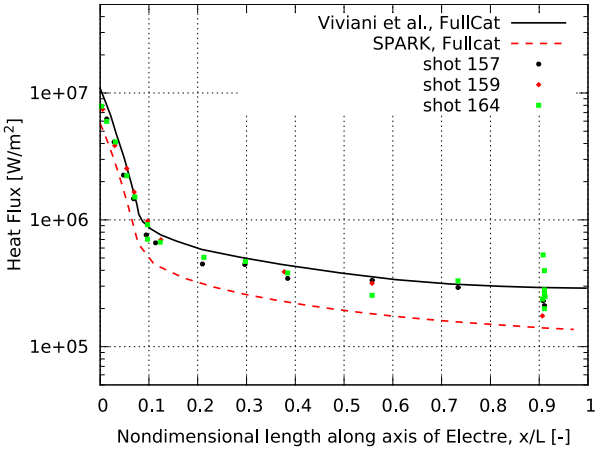

Figure 9: Total Heat Flux onto Electre - $\gamma = 1$. SPARK results vs. Viviani et al. [13]. The "shots" correspond to experimental data.

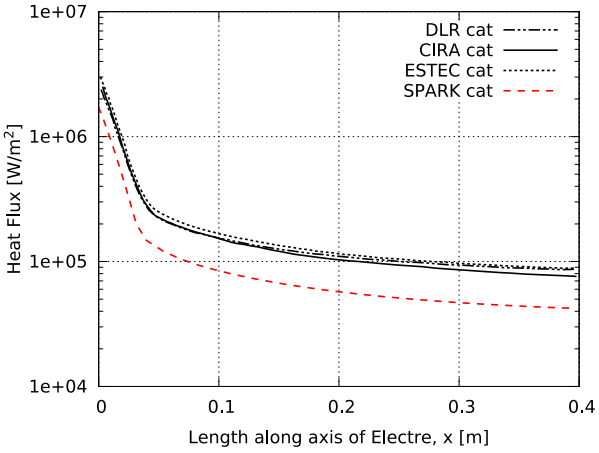

Figure 10: Total Heat Flux onto Electre - $\gamma = 1$. SPARK results vs. Muylaert et al. [11]. DLR, CIRA and ESTEC are independent CFD codes.

On their work, Muylaert et al. present results from three different CFD codes which are as similar, from a CFD point of view, between each other as they are to SPARK.
Despite this diversity, all the 3 codes agree to a large extent for the full catalytic simulation, figure 10, while SPARK underpredicts those curves along the entire surface. At the nose of Electre the difference to the CIRA curve is 33% and at x = 0.4 m is about 50 %. This results show that the differences presented by SPARK cannot be justified by it using models (chemical reaction set, procedure to evaluate the diffusion coefficient D_i etc.) different from the benchmarking codes. Otherwise the CIRA, DLR and ESTEC codes, which do not share many features, would present a higher dispersion between each other.

6. Finite-Rate Surface Chemistry model

The next step towards a state-of-the-art modelling of catalycity is a general finite-rate surface chemistry (FRSC) model. The improvement consists in abandoning the imposed surface efficiency γ, that attempts to macroscopically model catalycity and start taking into account the microscopic processes responsible, on a more basic level, for catalycity. This processes take the form of elementary surface reactions, such as:

$$\begin{aligned} &\text{Adsorption:} && \mathrm{A} + (\mathrm{s}) \rightleftharpoons \mathrm{A(s)} \\ &\text{Eley-Rideal:} && \mathrm{B} + \mathrm{A(s)} \rightleftharpoons \mathrm{AB} + (\mathrm{s}) \\ &\text{Langmuir-Hinshelwood:} && \mathrm{A(s)} + \mathrm{B(s)} \rightleftharpoons \mathrm{AB} + 2\,(\mathrm{s}) \end{aligned} \tag{17}$$

Where A, B and AB are gas species and (s), A(s) and B(s) are surface species.
All the reactions are written in the form:

$$\sum_{i=1} \nu_{ir}^{'} A_i \longleftrightarrow \sum_{i=1} \nu_{ir}^{''} A_i \tag{18}$$

On this work, this model was not incorporated into SPARK. Instead, a stand-alone code was developed that models surface reactions decoupled from the main fluid flow. In other others, it is able to compute the steady state composition of all species in a system, when this system is allowed to adjust solely via the said surface reactions, at a given temperature and pressure, from a given initial condition.
The objective was to prepare for a future implementation in SPARK, on which the current mass balance equation in the form of (4) is mantained but, at each CFD iteration, instead of evaluating the production terms via expressions (8) and (9), this stand-alone code is used to compute the production terms of the gas species via the FRSC model, where the production terms are now given by:

$$\dot{w}_{ir} = (\nu_{ir}^{''} - \nu_{ir}^{'}) \left\{ k_{fr} \prod_{i=1} X_i^{\nu_{ir}^{''}} - k_{br} \prod_{i=1} X_i^{\nu_{ir}^{''}} \right\} \tag{19}$$

Where k_{fr} and k_{br} are reaction rates of a surface reaction r and X_i is the concentration of species i. The results of the developed stand-alone code, not shown here, were compared with the work of MacLean et al. [8] and, for the cases analysed, there is a perfect agreement.

7. Conclusions

Before the current work, SPARK did not have the capability to account for catalycity in re-entry simulations. The current work implemented catalycity in SPARK for Earth re-entry following a phenomenological approach. Through it, two catalytic reactions are accounted for: N_2 and O_2 recombination. Modelling them consists in recognizing a

parameter, the reaction efficiency γ, that quantifies the ratio of the incoming N and O atoms that achieve recombination.
The account of surface reactions at the surface required a mass and energy balance at the wall which was not done before in SPARK. From the energy balance point of view two alternatives were implemented. One for constant wall temperature T_w and the other for radiative equilibrium. To verify and validate the implementation a battery of simulations were ran and the results compared with several other computational codes and experimental data. Given the results, doubts remain on whether the implementation was successful. Further analysis is needed.
The author suspects that the computation of Δn, used from expression (11) onward, and which must account for metric terms resulting from the overall discretization scheme followed by SPARK, is incorrect. Ideally this question could be answered by analysing the theoretical implementation of boundary conditions in similar aerothermodynamics CFD codes.
In what concerns with the FRSC model, the work developed is a preliminary step before the full implementation in SPARK. From that point of view, the results obtained were in good agreement the work of MacLean et al. [8].

References

[1] H. Alkandry, E. D. Farbar, and I. D. Boyd. Evaluation of finite-rate surface chemistry models for simulation of the stardust reentry capsule. *AIAA 2012-2874*.

[2] M. Barbato, D. Giordano, and C. Bruno. Comparison between finite rate and other catalytic boundary conditions for hypersonic flows. *AIAA 94-2074*, 1994. 6$^{\text{th}}$ AIAA/ASME Joint Thermophysics and Heat Transfer Conference, June 20-23, 1994/Colorado Springs, CO.

[3] D. Bianchi. *Modeling of ablation phenomena in space applications*. PhD thesis, Universit degli Studi di Roma "La Sapienza", Dipartimento di Meccanica e Aeronautica, 2006/2007.

[4] P. A. Gnoffo. Planetary-entry gas dynamics. *Annual Review of Fluid Mechanics*, 31:459–494, 1999.

[5] W. L. Hankey. *Re-entry Aerodynamics*. AIAA Educational Series, 1988.

[6] M. MacLean, J. Marschall, and D. M. Driver. Finite-rate surface chemistry model, ii: Coupling to viscous navier-stokes code. *AIAA 2011-3784*.

[7] J. Marschall. Laboratory determination of thermal protection system materials surface caatlytic properties. In *TRO-EN-AVT-142, Paper 11*.

[8] J. Marschall and M. MacLean. Finite-rate surface chemistry model, i: Formulation and reaction system examples. *AIAA 2011-3783*.

[9] J. H. Miller, J. C. Tannehill, G. Wadawadigi, T. A. Edwards, and S. L. Lawrence. Computation of hypersonic flows with finite-catalytic walls. In 25^{th} *AIAA Fluid Dynamics Conference, June 20-23/1994 Colorado Springs, CO*, number AIAA 94-2354.

[10] F. S. Milos and D. J. Rasky. Review of numerical procedures for computational surface thermochemistry. *Journal of Thermophysics and Heat Transfer*, 8(1), January-March 1994.

[11] J. Muylaert, L. Walpot, M. Spel, P. Sagnier, K. Hannemann, and H. Olivier. A review of european code validation studies in high enthalpy flow. *American Institute of Aeronautics and Astronautics, Inc.*, (98-2769), 1998.

[12] C. D. Scott. Wall boundary equations with slip and catalysis for multicomponent nonequilibrium gas flows. NASA TM X-58111, December 1973.

[13] A. Viviani and G. Pezzella. Nonequilibrium aerothermodynamics for a capsule reentry vehicle. In *Engineering Applications of Computational Fluid Mechanics*, volume 3, pages 543–561. 2009.